AUTOMATIC DETECTION AND SEGMENTATION OF ABDOMINOPELVIC LYMPH NODES ON COMPUTED TOMOGRAPHY SCANS

Jiamin Liu, Chin-Hsiang Feng, Jeremy Hua, Jianhua Yao, Jacob M. White, Ronald M. Summers

Imaging Biomarkers and Computer-aided Diagnosis Laboratory
Radiology and Imaging Sciences, National Institutes of Health Clinical Center
Building 10 Room 1C224 MSC 1182, Bethesda, MD 20892-1182

ABSTRACT

We proposed a local scale-based Hessian analysis method for automated lymph node detection in contrast-enhanced abdominopelvic CT scans. First, spine and pelvic girdle were automatically segmented to locate the abdominopelvic region. Blood vessels were then segmented to narrow the search region to the perivascular space where lymph nodes are located. Lymph node candidates were generated by scale-based Hessian analysis. The detected candidates were segmented by curve evolution. Characteristic features were calculated on the segmented nodes. Support vector machine was utilized for classification and false positive reduction. We applied our method to 22 patients with 37 enlarged lymph nodes. The system achieved 83% sensitivity at 5 false positives per patient. Our results indicated that computer-aided abdominopelvic lymph node detection is feasible with a high sensitivity and a relatively low FP rate.

Index Terms **—** lymph node detection, Hessian matrix, object scale

1. INTRODUCTION

Abdominopelvic lymphadenopathy is found commonly in many diseases. Lymphoma and metastatic disease are two example diseases often associated with abdominopelvic lymphadenopathy [1]. According to the RECIST guidelines [2], a lymph node is considered enlarged (swollen) if it is more than 10 mm in diameter on computed tomography (CT). It is important to detect and track over time enlarged lymph nodes on serial images to assess therapeutic response.

Lymph node analysis is a significant part of daily clinical work in radiology. Lymph nodes near primary cancer regions are routinely assessed by clinicians for accurate staging, prognosis, choice of proper therapy, and follow-up of oncology patients. The assessment is usually based on CT images. In the current clinical workflow, radiologists and other physicians have to detect, quantitatively evaluate and classify lymph nodes by manually examining all slices of CT scans. This process can be very time consuming and error-prone. Therefore, a system for automated lymph node detection and measurement is desired.

Approaches for the segmentation of lymph nodes on CT have been presented by several researchers. Rogowska et al. [3] evaluated elementary segmentations such as thresholding and watershed transformation for lymph node segmentation and concluded that a high degree of model knowledge is needed for a reliable segmentation. Honea et al. [4, 5] used active contours and Yan et al. [6] applied the fast marching method for lymph node segmentation. Dornheim et al. [7] proposed a stable 3D mass-spring model for segmentation of neck lymph nodes. Gorthi et al. [8] presented the segmentation of head and neck lymph node regions using an atlas registration model.

Little work has been done on the automated detection of lymph nodes. Kitasaka et al. [9] proposed a 3D minimum directional difference filter for automated detection of lymph nodes on abdominal CT images. Barbu et al. [10] proposed a machine learning based method for detection and segmentation of axillary and pelvic lymph nodes on CT images. Feuerstein [11] proposed Hessian analysis for automated detection of lymph nodes on contrast-enhanced chest CT images.

Object scale proposed by Saha et al. [12, 13] is a fundamental, well-established concept in image processing. The concept of object scale considers the local size of the object on the image. This local size concept motivates us to consider object scale in a Hessian analysis for blob-like node detection.

In this paper, we propose a scale-based Hessian analysis method for automated lymph node detection on contrast-enhanced abdominopelvic CT images. The detection response measure, blobness, is defined based on Hessian analysis and a local object scale [12, 13]. Voxels with higher blobness are clustered as lymph node candidates. Then, the detected potential candidates are segmented by curve

evolution [14]. Finally, features are calculated on the segmented candidates and support vector machines (SVM) classification is utilized for false positive reduction.

The complete methodology of our approach is described in Section 2. We demonstrate in Section 3 both visually and quantitatively the effectiveness. Our concluding remarks are stated in Section 4.

2. METHODS

The method consists of four stages: (1) spine extraction, (2) vessel segmentation, (3) lymph nodes candidate detection, and (4) lymph node segmentation, feature computation and selection for classification and false-positive reduction.

2.1. Spine and pelvic girdle segmentation

The system is designed to run on contrast-enhanced chest/abdominal/pelvis CT images. Therefore, in the first stage, the spine and pelvic girdle are automatically extracted based on adaptive thresholding, morphologic operations and region growing [15]. The lower half of the segmented spine and the entirety of the pelvic girdle indicate the abdominopelvic region. Figure 1 shows one example of extracted spine and pelvic girdle.

2.2. Vessel segmentation

In the second stage, blood vessels (abdominal aorta, common iliac artery, internal and external iliac arteries) are segmented using fuzzy connectedness [12]. Hough transform is utilized to automatically find the center of the aorta. This center is used as the seed point for vessel segmentation (Figure 1). The search region for lymph nodes is then defined by dilating the segmented vessel by a square.

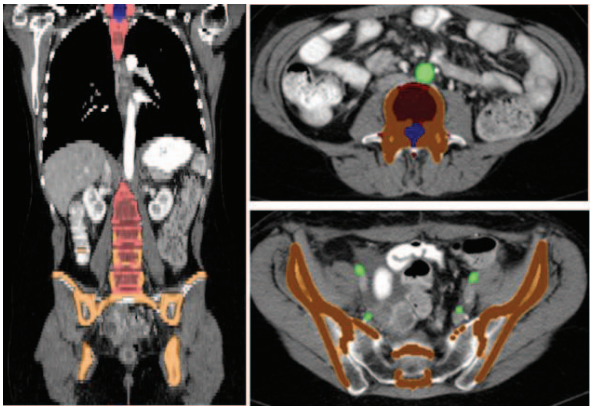


Figure 1. Extracted spine (red) and pelvic girdle (brown) and vessels (green) .

2.3. Lymph nodes candidate detection and segmentation

2.3.1. Scale computation

In the third stage, a local object scale [12] is computed at every voxel in the search region. The object scale $k(c)$ at every voxel c, is defined as the radius of the largest hyperball centered at the voxel c such that all voxels within the ball satisfied a predefined image intensity homogeneity criterion. First, for any voxel c in a given image, a digital ball of radius r centered at c is the set of voxels,

$$B_r(c) = \{d \mid \|d - c\| \le r\}, \tag{1}$$

where $\|d - c\|$ denotes the distance between voxel c and d. Then, a homogeneity fraction, $FO_r(c)$, is defined, that indicates the fraction of the ball boundary occupied by a region which is sufficiently homogeneous with c by

$$FO_r(c) = \frac{\sum_{d \in B_r(c)} W(f(c) - f(d))}{|B_r(c) - B_{r-1}(c)|}, \tag{2}$$

where $|B_r(c) - B_{r-1}(c)|$ is the number of voxels (i.e., volumes of) in $B_r(c) - B_{r-1}(c)$, $f(c)$ is the intensity of voxel c, and $W(x)$ is a homogeneity function defined by

$$W(x) = e^{-\frac{x^2}{2}}. \tag{3}$$

The algorithm of scale computation initializes $k(c)$ at every voxel c as 1. Then it iteratively increases the ball radius r by 1, and checks for the fraction of the object $FO_r(c)$ containing c that is contained in the ball. The first time when this fraction falls below a predefined constant, we consider that the ball contains an object region different from that to which c belongs and set $k(c)$ as r. Further details can be found in [12].

2.3.2. Scale-based Hessian analysis

Then we compute the Hessian matrix for each voxel in the search region by convolution with the second and cross derivatives of a Gaussian with σ.

$$H_\sigma = \begin{vmatrix} I_{xx} & I_{xy} & I_{xz} \\ I_{yx} & I_{yy} & I_{yz} \\ I_{zx} & I_{zy} & I_{zz} \end{vmatrix} \tag{4}$$

$I(x,y,z)$ is the image intensity at voxel (x,y,z). The corresponding eigenvalues of H are λ_1, λ_2, λ_3, ($|\lambda_1| \le |\lambda_2| \le |\lambda_3|$). For each voxel, a blobness $B_\sigma(\lambda)$ detection response measure is defined as:

$$B_\sigma(\lambda)=\begin{cases}(1-e^{-R_A^2/2})(1-e^{-S^2/2})e^{-R_C^2/2} & \text{if } \lambda_i<0 \text{ for } i=1,2,3\\ 0 & \text{otherwise}\end{cases} \tag{5}$$

with

$$R_A=\frac{|\lambda_2|}{|\lambda_3|},$$

$$S=\sqrt{\lambda_1^2+\lambda_2^2+\lambda_3^2}\,, \tag{6}$$

$$R_C=k(c)-2\sigma\,.$$

The detection response $B_\sigma(\lambda)$ is defined between 0 and 1 and will be maximum when σ and the actual size (radius) of the blob to detect approximately match (i.e. $k(c)=2r$). Ideally, the center of the blob has the maximal detection response.

The σ subscript in B_σ indicates that blobness is computed on a smoothed version of the image and is therefore representative of the variations of image intensity at the spatial scale σ. In our application, blobness is evaluated at σ=2.5, 3.5 and 4.5 mm, and finally the maximum response $B_\sigma(\lambda)$ is selected for every voxel:

$$B(\lambda)=\max_{\sigma\in\{2.5,3.5,4.5\}} B_\sigma(\lambda) \tag{7}$$

Since voxels with higher blobness are likely to be lymph nodes, voxels with $B(\lambda)$ ≥0.2 are clustered based on connectivity and the clusters with at least 10 voxels are considered as potential lymph node candidates.

To remove common false positives such as muscles or organs, the algorithm shoots rays in 24 directions from each candidate's centroid. These 24 directions include 8 directions (every 45 degree) in three orthogonal planes. In each direction, local maxima of the gradient is computed and those detected candidates with longer z direction (muscles) or candidates with non-symmetric rays in xy direction (organs) are removed from the detection list.

2.4 Segmentation of lymph node candidates and false-positive reduction

The detected candidates are segmented using curve evolution [14] where the centroid of each candidate provides the initial curve. As the Hessian analysis produces many false positive lymph node candidates, characteristic features, such as intensity, volume, curvatures, and shape-related features are calculated for the segmented candidates. Support vector machine (SVM) classification is applied for false positive reduction.

3. RESULTS

The patient population consisted of 22 patients with enlarged abdominopelvic lymph nodes on intravenous contrast-enhanced CT images . The use of the data was IRB-approved. Each patient had at least one lymph node measuring 10 mm or greater in diameter. A medical student under the supervision of a radiologist manually traced 37 lymph nodes (21 mm ± 6.8 mm) to form the reference standard.

Performance of scale-based Hessian analysis was evaluated and compared with Frangi's [16] and Li's [17] blobness methods. These two blobness methods are also based on Hessian analysis and are comparable to our method. The system using our scale-based Hessian analysis achieved 83% sensitivity at 5 false positives per patient. The system achieved 68% and 52% sensitivities at 5 false positive per patient for Frangi's and Li's blobness, respectively. Figure 2 shows the 10-fold cross validation free response receiver operating characteristic (FROC) curves for the three methods. Examples of the search region, a false positive removed by the ray shooting and a detected lymph node are shown in Figure 3.

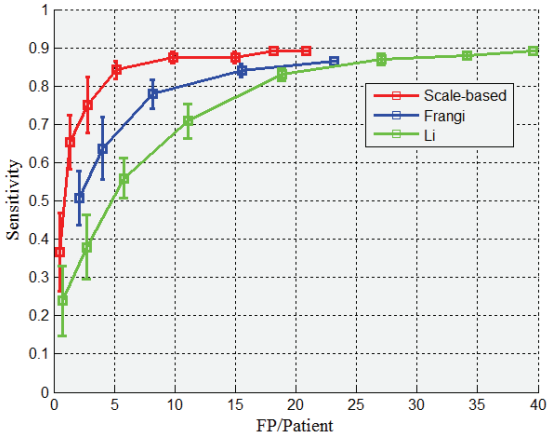


Figure 2. 10-fold cross validation FROC of three blobness methods: our scale-based (red), Frangi's (blue) and Li's (green).

4. DISCUSSION AND CONCLUSIONS

In this paper, we presented a scale-based Hessian analysis method for automated abdominopelvic lymph node detection on CT images. Local structure by object scale and shape discrimination by Hessian analysis are simultaneously considered in the detection response measure.

The detection of single or isolated blobs is not difficult. Detection is more complicated when blobs and other structures are very close to each other, which is normal in biomedical images. This is because the smoothing during the

multi-scale Hessian analysis blurs the boundaries too much and thus causes a strong detection response in the close-by boundary regions. The new method proposed in this paper overcame this problem by introducing an object scale-based term $e^{-R_c^2/2}$ in the blobness definition (eq. (5)). This term produces a weak detection response in those regions and diminishes this problem.

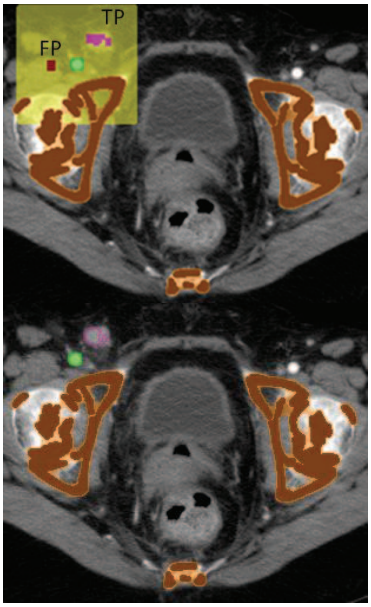


Figure 3. Example of lymph node detection. True and false positive detections in the pelvis are shown. The 3D ray tracing eliminated the false positive on a normal muscle. The segmented lymph node (pink), pelvic girdle (brown) and search region (yellow) are also shown.

Many false positives arise from the muscle, intestines, and other organs. Therefore, in the future, in addition to blood vessels, organs will be included as other important biomarkers for lymph node detection. For example, segmentation of organs could be utilized to limit search region. In the false positive reduction stage, the detection candidate will be considered as false positive if 5% of its volume falls within the extracted organs.

In summary, our scale-based detection algorithm is accurate for automated lymph node detection in abdominopelvic CT images. CAD with this method may yield a high sensitivity and a relatively low FP rate.

5. ACKNOWLEDGMENT

This research was supported by the Intramural Research Program of the NIH Clinical Center.

REFERENCE

[1] D. M. Einstein, et al., "Abdominal lymphadenopathy: spectrum of CT findings," Radiographics, 1991. **11**(3): pp. 457-72.

[2] Therasse, P., et al., "New guidelines to evaluate the response to treatment in solid tumors. European Organization for Research and Treatment of Cancer, National Cancer Institute of the United States, National Cancer Institute of Canada," J Natl Cancer Inst, 2000. **92**(3): pp. 205-16.

[3] Rogowska, J., et al., "Evaluation of selected two-dimensional segmentation techniques for computed tomography quantitation of lymph nodes," Invest Radiol, 1996. **31**(3): pp. 138-45.

[4] Honea, D., et al., "Lymph node segmentation using active contours," In Proceedings of SPIE, 1997. **3034**: pp. 165-273.

[5] Honea, D. and W. Snyder, "Three-dimensional active surface approach to lymph node segmentation," In Proceedings of SPIE, 1999. **3361**: pp. 1003-1011.

[6] Yan, J., et al., "Lymph node segmentation from CT images using fast marching method," Comput Med Imaging Graph, 2004. **28**(1-2): p. 33-8.

[7] Dornheim, J., et al., "Segmentation of neck lymph nodes in CT datasets with stable 3D mass-spring models," Med Image Comput Comput Assist Interv, 2006. **9**(Pt 2): pp. 904-11.

[8] Gorthi, S., et al., "Segmentation of head and neck lymph node regions for radiotherapy planning, using active contour based atlas registration," IEEE Journal of selected topics in signal processing, 2009. **3**: pp. 135-147.

[9] Kitasaka, T., et al., "Automated extraction of lymph nodes from 3-D abdominal CT images using 3-D minimum directional difference filter," Med Image Comput Comput Assist Interv, 2007. **10**(Pt 2): pp. 336-43.

[10] Barbu, A., et al., "Automatic detection and segmentation of axillary lymph nodes," Med Image Comput Comput Assist Interv. **13**(Pt 1): pp. 28-36.

[11] Feuerstein, I.M., et al., "Automatic mediastinal lymph node detection in chest CT," In Proceedings of SPIE, 2009. **7260**: pp. 72600V-72600V11.

[12] Saha, P.K., J.K. Udupa, and D. Odhner, "Scale-based fuzzy connected image segmentation: theory, algorithms, and validation," Computer Vision and Image Understanding, 2000. **77**: pp. 145-174.

[13] Saha, P.K. and J.K. Udupa, "Scale-based image filtering preserving boundary sharpness and fine structure," IEEE Transactions on Medical Imaging 2001. **20**: pp. 1140-1155.

[14] Y. Shi and W. Karl. "A fast level set method without solving PDEs," in IEEE International Conference Acoustics Speech and Signal Processing. 2005. Philadelphia, PA.

[15] Yao, J., S.D. O'Connor, and R.M. Summers. "Automated spinal column extraction and partitioning," in 2006 3rd IEEE International Symposium on Biomedical Imaging: From Nano to Macro - Proceedings. 2006.

[16] Frangi, A., et al., "Multiscale vessel enhancement filtering," Lecture Notes in Computer Science, 1998. **1496**: pp. 130-137.

[17] Q. Li, S. Sone, and K. Doi, "Selective enhancement filters for nodules, vessels, and airway walls in two- and three-dimensional CT scans." Medical Physics, 2003. **30**: pp. 2040-51.